Sub-wavelength sensing of bi-periodic materials using topological sensitivity of second-order homogenized model

Marc Bonnet, Rémi Cornaggia, Bojan B Guzina

Sub-wavelength sensing of bi-periodic materials using topological sensitivity of second-order homogenized model

IOP Conf. Series: Journal of Physics: Conf. Series **1131** (2018) 012008 doi:10.1088/1742-6596/1131/1/012008

Sub-wavelength sensing of bi-periodic materials using topological sensitivity of second-order homogenized model

Marc Bonnet[1], **Rémi Cornaggia**[2] **and Bojan B Guzina**[3]

[1] POems (UMR 7231 CNRS-INRIA-ENSTA), ENSTA, Palaiseau, France
[2] Univ Rennes, CNRS, IRMAR - UMR 6625, F-35000 Rennes, France
[3] Department of Civil, Environmental and Geo-Engineering, University of Minnesota, Twin Cities, USA

E-mail: remi.cornaggia@univ-rennes1.fr

Abstract. We aim to detect defects or perturbations of periodic media, e.g. due to a defective manufacturing process. To this end, we consider scalar waves in such media through the lens of a second-order macroscopic description, and we compute the sensitivities of the germane effective parameters due to topological perturbations of a microscopic unit cell. Specifically, our analysis focuses on the tensorial coefficients in the governing mean-field equation – including both the leading order (i.e. quasi-static) terms, and their second-order companions bearing the effects of incipient wave dispersion. Then, we present a method that permits sub-wavelength sensing of periodic media, given the (anisotropic) phase velocity of plane waves illuminating the considered medium for several angles and wavenumbers.

1. Introduction

The sensitivity of an homogeneous material to the nucleation of a periodic array of inhomogeneities, and the computation of the corresponding homogenized coefficient, are well-addressed issues, see e.g. [1] and the references therein. By contrast, the sensitivity of an *already periodic* material to an additional periodic perturbation has been studied quite recently, and is mostly used to direct optimization procedures, see e.g. [4] for in-plane elastostatics. Moreover, the focus is often put on static (or quasi-static) configurations, for which the leading-order homogenized coefficients provides a valuable insight of the macroscopic behavior of the fields of interest.

In this study, we assume time-harmonic conditions, and aim at performing *sub-wavelength* sensing of periodic media, i.e. using low-frequency probing waves to detect defects or perturbations of the medium. This goal is achieved by relying on the *anisotropic dispersive properties* of such medium. To capture these properties, we chose to deploy the *second-order model* obtained by two-scale asymptotic homogenization [5], and we compute the sensitivities of the (tensor-valued) coefficients of the corresponding wave equation.

This model, and the corresponding sensitivities, are presented in Section 2. A sub-wavelength sensing method is then developed in Section 3, and applied to the probing of a defective checkerboard-like material. These results are finally summarized in Section 4.

2. Topological sensitivity of second-order homogenized model

Consider an elastic material occupying a 2D domain and characterized by periodic shear modulus μ and density ρ. The unit cell Y has characteristic length ℓ. Under time-harmonic conditions at circular frequency ω, the antiplane displacement u satisfies the wave equation:

$$\boldsymbol{\nabla} \cdot (\mu \boldsymbol{\nabla} u) + \omega^2 \rho u = 0$$

For long-wavelength configurations (i.e. $\ell \ll \lambda$), two-scale periodic homogenization of this equation [5] leads to the equation satisfied by the mean field U:

$$\boldsymbol{\mu}^0 : \boldsymbol{\nabla}^2 U + \omega^2 \varrho^0 U = -\ell^2 \left[\boldsymbol{\mu}^2 : \boldsymbol{\nabla}^4 U + \omega^2 \boldsymbol{\varrho}^2 : \boldsymbol{\nabla}^2 U \right] + o(\ell^3), \tag{1}$$

where the leading-order and second-order homogenized coefficients $(\boldsymbol{\mu}^0, \varrho^0, \boldsymbol{\mu}^2, \boldsymbol{\varrho}^2)$ are constant tensors, $\boldsymbol{\nabla}^k U$ stands for the k-th gradient of U and ":" denote the inner product of two tensors (i.e. the full contraction over all their indices).

This study considers a periodic perturbation of this material, whereby a penetrable inhomogeneity B_a, of size a and shape $\mathcal{B}$, characterized by contrasts $(\Delta\mu, \Delta\rho)$ is introduced at point $\boldsymbol{z} \in Y$ (Fig. 1). Then, the leading-order expansion of the perturbed coefficients $(\boldsymbol{\mu}_a^0, \varrho_a^0, \boldsymbol{\mu}_a^2, \boldsymbol{\varrho}_a^2)$ w.r.t. a are computed, following previous studies e.g. [4] for in-plane elastostatics.

2.1. Leading-order coefficients

Let $\langle \cdot \rangle = |Y|^{-1} \int_Y \cdot$ denote an average on the unit cell. The homogenized density ϱ^0 is defined by $\varrho^0 = \langle \rho \rangle$, so that the perturbed coefficient ϱ_a^0 and the *topological sensitivity* $\mathcal{D}\varrho^0$ are exactly given by:

$$\varrho_a^0 = \varrho^0 + a^2 |Y|^{-1} \mathcal{D}\varrho^0, \quad \text{with } \mathcal{D}\varrho^0 = |\mathcal{B}| \Delta\rho.$$

The homogenized shear modulus $\boldsymbol{\mu}^0$ is defined by $\boldsymbol{\mu}^0 = \langle \mu(\boldsymbol{I} + \boldsymbol{\nabla}\boldsymbol{P}) \rangle^{\mathrm{S}}$, where $\boldsymbol{I}$ is the identity tensor, the first *cell function* $\boldsymbol{P}$ [5] is the Y-periodic and zero-mean vector-valued solution of:

$$\boldsymbol{\nabla} \cdot (\mu(\boldsymbol{I} + \boldsymbol{\nabla}\boldsymbol{P})) = \boldsymbol{0} \tag{2}$$

and the superscript $\cdot^{\mathrm{S}}$ means symmetrization w.r.t. all index permutations. Consequently, $\boldsymbol{\mu}_a^0$ is computed as:

$$\boldsymbol{\mu}_a^0 = \boldsymbol{\mu}^0 + \langle \mu \boldsymbol{\nabla} \boldsymbol{p}_a \rangle^{\mathrm{S}} + \langle \chi_{B_a} \Delta\mu (\boldsymbol{I} + \boldsymbol{\nabla}\boldsymbol{P}_a) \rangle^{\mathrm{S}}$$

where $\boldsymbol{p}_a := \boldsymbol{P}_a - \boldsymbol{P}$ is the perturbation of $\boldsymbol{P}$ and χ_{B_a} is the characteristic function of B_a. The analysis of this perturbation is done by reformulating problem (2) and its perturbed counterpart using domain integral equations, in the spirit of e.g. [2]. With the help of the adjoint state method, it leads to the following leading-order expansion:

$$\boldsymbol{\mu}_a^0 = \boldsymbol{\mu}^0 + a^2 |Y|^{-1} \mathcal{D}\boldsymbol{\mu}^0(\boldsymbol{z}) + o(a^2 |Y|^{-1}), \tag{3}$$

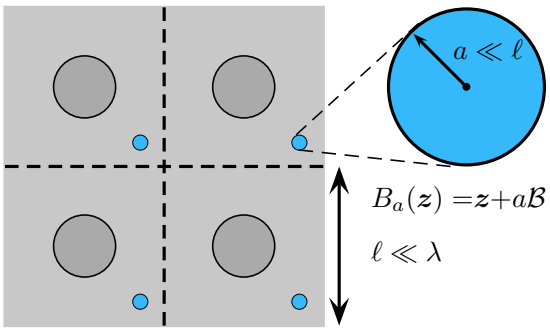

Figure 1: *Notation for a bi-periodic material whose unit cell is perturbed by an inhomogeneity B_a*

with the topological derivative $\mathcal{D}\boldsymbol{\mu}^0$ given by:

$$\mathcal{D}\boldsymbol{\mu}^0(\boldsymbol{z}) = \left[(\boldsymbol{I}+\boldsymbol{\nabla P})\cdot\boldsymbol{A}\cdot(\boldsymbol{I}+\boldsymbol{\nabla P})^{\mathrm{T}}\right](\boldsymbol{z}) \tag{4}$$

where $\boldsymbol{A}(\boldsymbol{z}) = \boldsymbol{A}(\mathcal{B}, \mu(\boldsymbol{z}), \Delta\mu)$ is the *polarization tensor* [1] associated to shape $\mathcal{B}$ and moduli $\mu(\boldsymbol{z})$ and $\mu(\boldsymbol{z})+\Delta\mu$. Under notational adjustments, this result is similar to [4]. For homogeneous background materials, in which case $\boldsymbol{P}=\boldsymbol{0}$, one obtains $\mathcal{D}\boldsymbol{\mu}^0 = \boldsymbol{A}$ as shown by [1].

2.2. Second-order coefficients

The second-order homogenized density is defined by $\boldsymbol{\varrho}^2 = \langle\rho\boldsymbol{Q}\rangle^{\mathrm{S}}$, where the *second cell function* $\boldsymbol{Q}$ is the Y-periodic, zero-mean, tensor-valued solution of:

$$\boldsymbol{\nabla}\cdot(\mu(\boldsymbol{P}\otimes\boldsymbol{I}+\boldsymbol{\nabla Q})) = -\mu(\boldsymbol{I}+\boldsymbol{\nabla P}) + (\rho/\varrho^0)\boldsymbol{\mu}^0 \tag{5}$$

Relying on the same integral equation framework, and with careful analysis of the influence of the source terms involving $\boldsymbol{P}_a$ when adressing the perturbed cell function $\boldsymbol{Q}_a$, we show that $\boldsymbol{\varrho}_a^2$ has an expansion of the same form as (3), with its topological derivative $\mathcal{D}\boldsymbol{\varrho}^2$ given by:

$$\begin{aligned}\mathcal{D}\boldsymbol{\varrho}^2(\boldsymbol{z}) = \Big[&(\boldsymbol{I}+\boldsymbol{\nabla P})\cdot\boldsymbol{A}\cdot\Big(\beta\boldsymbol{I}+\boldsymbol{\nabla}\hat{\boldsymbol{X}}[\beta]\Big)^{\mathrm{T}} - (\boldsymbol{P}\otimes\boldsymbol{I}+\boldsymbol{\nabla Q})\cdot\boldsymbol{A}\cdot\boldsymbol{\nabla}\beta \\ &- \left(\mathcal{D}\boldsymbol{\mu}^0 - (\mathcal{D}\varrho^0/\varrho^0)\boldsymbol{\mu}^0\right)\langle\rho(\beta/\varrho^0)\rangle - \mathcal{D}\varrho^0\left((\beta/\varrho^0)\boldsymbol{\mu}^0 - \boldsymbol{Q}\right)\Big]^{\mathrm{S}}(\boldsymbol{z}).\end{aligned} \tag{6}$$

The above expression features (i) various combinations of the previously computed cell solutions and topological derivatives and (ii) two new *adjoint fields* β and $\hat{\boldsymbol{X}}[\beta]$ defined as the (Y-periodic, zero-mean) solutions of:

$$\boldsymbol{\nabla}\cdot(\mu\boldsymbol{\nabla}\beta) = -(\rho-\varrho^0) \quad\text{and}\quad \boldsymbol{\nabla}\cdot(\mu(\beta\boldsymbol{I}+\boldsymbol{\nabla}\hat{\boldsymbol{X}}[\beta])) = -\mu\boldsymbol{\nabla}\beta. \tag{7}$$

The second-order homogenized shear modulus is defined by $\boldsymbol{\mu}^2 = \langle\mu(\boldsymbol{Q}\otimes\boldsymbol{I}+\boldsymbol{\nabla R})\rangle^{\mathrm{S}}$ in terms of $\boldsymbol{Q}$ and a third cell function $\boldsymbol{R}$, the Y-periodic, zero-mean solution of:

$$\boldsymbol{\nabla}\cdot(\mu(\boldsymbol{Q}\otimes\boldsymbol{I}+\boldsymbol{\nabla R})) = -\mu(\boldsymbol{I}\otimes\boldsymbol{P}+\boldsymbol{\nabla Q}) + (\rho/\varrho^0)\boldsymbol{P}\otimes\boldsymbol{\mu}^0 \tag{8}$$

Once again, an analysis of the problems satisfied by $\boldsymbol{R}$ and $\boldsymbol{R}_a$ is conducted. As a result, $\boldsymbol{\mu}_a^2$ is found to have an expansion similar to (3), and its topological derivative $\mathcal{D}\boldsymbol{\mu}^2$ is:

$$\begin{aligned}\mathcal{D}\boldsymbol{\mu}^2(\boldsymbol{z}) = &\Big\{2\left(\boldsymbol{\nabla P}+\boldsymbol{I}\right)^{\mathrm{T}}\cdot\boldsymbol{A}\cdot(\boldsymbol{\nabla R}+\boldsymbol{I}\otimes\boldsymbol{Q}) - (\boldsymbol{\nabla Q}+\boldsymbol{I}\otimes\boldsymbol{P})^{\mathrm{T}}\cdot\boldsymbol{A}\cdot(\boldsymbol{\nabla Q}+\boldsymbol{I}\otimes\boldsymbol{P})\Big\}^{\mathrm{S}}(\boldsymbol{z}) \\ &+\left\{\left[\mathcal{D}\boldsymbol{\varrho}^2 + \mathcal{D}\varrho^0(\boldsymbol{P}\otimes\boldsymbol{P}-2\boldsymbol{Q})\right]\otimes\frac{\boldsymbol{\mu}^0}{\varrho^0} + \frac{1}{\varrho^0}\left(\langle\rho\boldsymbol{P}\otimes\boldsymbol{P}\rangle - \boldsymbol{\varrho}^2\right)\otimes\left(\mathcal{D}\boldsymbol{\mu}^0 - \mathcal{D}\varrho^0\frac{\boldsymbol{\mu}^0}{\varrho^0}\right)\right\}^{\mathrm{S}}(\boldsymbol{z}).\end{aligned} \tag{9}$$

Remark that the fields $(\boldsymbol{P}, \boldsymbol{Q}, \boldsymbol{R}, \beta, \hat{\boldsymbol{X}}[\beta])$, which are involved in the expressions (4,6,9) of the topological sensitivities, solve the problems (2,5,8,7) which are all posed on the *unperturbed* cell.

3. Sub-wavelength sensing of periodic materials

We now present a *defect identification* procedure, where a "defective" checkerboard material (hereon called the *manufactured* material) is interrogated by plane waves. The sensory data, used to probe for defects, are the phase velocities of such waves for several incidence directions, as captured over a low-frequency (and thus long-wavelength) range. In the identification procedure, the experimental phase velocities are compared to their reference values, computed for the *designed* material. The observed anisotropic dispersion, a key feature of the sensory data, is captured only via *second-order* homogenization, so that both zero-order ($\mathcal{D}\varrho^0$, $\mathcal{D}\boldsymbol{\mu}^0$) and second-order ($\mathcal{D}\boldsymbol{\varrho}^2$, $\mathcal{D}\boldsymbol{\mu}^2$) coefficient sensitivities are needed to interpret the data.

3.1. Topological sensitivity of the phase velocity
We first recall the second-order, mean field equation

$$\boldsymbol{\mu}^0 : \boldsymbol{\nabla}^2 U + \ell^2 \boldsymbol{\mu}^2 : \boldsymbol{\nabla}^4 U + \omega^2 \left(\varrho^0 U + \ell^2 \boldsymbol{\varrho}^2 : \boldsymbol{\nabla}^2 U \right) \;=\; o(\ell^3), \tag{10}$$

according to (1). To characterize the dispersion of a homogenized material, we set the mean field as a plane wave propagating in direction $\boldsymbol{d} = (\cos\theta, \sin\theta)$ with wavenumber k, i.e. $U(\boldsymbol{x}) \propto e^{\mathrm{i}k\boldsymbol{d}\cdot\boldsymbol{x}}$. On substituting this plane wave into (10) and neglecting the $o(\ell^3)$ remainder, one obtains the characteristic relation

$$\ell^2(\boldsymbol{\mu}^2 : \boldsymbol{d}^{\otimes 4})k^4 - \left((\boldsymbol{\mu}^0 + \ell^2\omega^2\boldsymbol{\varrho}^2) : \boldsymbol{d}^{\otimes 2}\right) k^2 + \omega^2 \varrho^0 \;=\; 0, \tag{11}$$

(with $\boldsymbol{d}^{\otimes 2} := \boldsymbol{d} \otimes \boldsymbol{d}$ and $\boldsymbol{d}^{\otimes 4} := \boldsymbol{d} \otimes \boldsymbol{d} \otimes \boldsymbol{d} \otimes \boldsymbol{d}$) which in turn yields the anisotropic dispersion formula

$$c(k, \boldsymbol{d}) \;=\; \frac{\omega(k, \boldsymbol{d})}{k} \;=\; \left(\frac{\boldsymbol{\mu}^0 : \boldsymbol{d}^{\otimes 2} - \ell^2 k^2 \boldsymbol{\mu}^2 : \boldsymbol{d}^{\otimes 4}}{\varrho^0 - \ell^2 k^2 \boldsymbol{\varrho}^2 : \boldsymbol{d}^{\otimes 2}} \right)^{1/2}. \tag{12}$$

For perturbed unit cells, the usual expansion $c_a = c + a^2 |Y|^{-1} \mathcal{D}c + o(a^2)$ holds, and $\mathcal{D}c$ is expressed in terms of the sensitivities of the homogenized coefficients:

$$\mathcal{D}c(k, \boldsymbol{d}, \boldsymbol{z}) = \frac{\left[\mathcal{D}\boldsymbol{\mu}^0 : \boldsymbol{d}^{\otimes 2} - \ell^2 k^2 \mathcal{D}\boldsymbol{\mu}^2 : \boldsymbol{d}^{\otimes 4} - (c(k, \boldsymbol{d}))^2 \left(\mathcal{D}\varrho^0 - \ell^2 k^2 \mathcal{D}\boldsymbol{\varrho}^2 : \boldsymbol{d}^{\otimes 2} \right) \right](\boldsymbol{z})}{2 \left(\varrho^0 - \ell^2 k^2 \boldsymbol{\varrho}^2 : \boldsymbol{d}^{\otimes 2} \right)}. \tag{13}$$

3.2. Quasi-static and dynamic misfit functionals
In what follows, the manufactured material is illuminated by plane waves with wavenumbers $(k_p)_{p=1..N_k}$ propagating in directions $(\theta_j)_{j=1..N_\theta}$. The sensory data are thus the phase velocities $c^{\mathrm{obs}}(k_p, \boldsymbol{d}_j)$, where $\boldsymbol{d}_j = (\cos\theta_j, \sin\theta_j)$. For given wavenumber and direction of incidence $(k, \boldsymbol{d})$, we define the cost functional

$$J(k, \boldsymbol{d}) \;=\; \frac{1}{2} \left[c(k, \boldsymbol{d}) - c^{\mathrm{obs}}(k, \boldsymbol{d}) \right]^2, \tag{14}$$

quantifying the misfit between the designed and observed phase velocities. We also define the dynamic cost functional J^{dyn}, extracting the effects of dispersion, as

$$J^{\mathrm{dyn}}(k, \boldsymbol{d}) \;=\; \frac{1}{2} \left[\Delta c(k, \boldsymbol{d}) - \Delta c^{\mathrm{obs}}(k, \boldsymbol{d}) \right]^2, \qquad \Delta c(k, \boldsymbol{d}) \;=\; c(k, \boldsymbol{d}) - c(k_{\min}, \boldsymbol{d}), \tag{15}$$

where $k_{\min}$ is the smallest observed wavenumber (typically, $k_{\min} = k_1 > 0$). The topological sensitivities of these two misfit functionals depend on the sensitivity $\mathcal{D}c$ given by (13) as

$$\begin{aligned} \mathcal{D}J(k, \boldsymbol{d}, \boldsymbol{z}) \;&=\; \Big(c(k, \boldsymbol{d}) - c^{\mathrm{obs}}(k, \boldsymbol{d}) \Big) \, \mathcal{D}c(k, \boldsymbol{d}, \boldsymbol{z}), \\ \mathcal{D}J^{\mathrm{dyn}}(k, \boldsymbol{d}, \boldsymbol{z}) \;&=\; \Big(\Delta c(k, \boldsymbol{d}) - \Delta c^{\mathrm{obs}}(k, \boldsymbol{d}) \Big) \left(\mathcal{D}c(k, \boldsymbol{d}, \boldsymbol{z}) - \mathcal{D}c(k_{\min}, \boldsymbol{d}, \boldsymbol{z}) \right), \end{aligned} \tag{16}$$

In this setting, we finally define the aggregate *quasistatic* and *dynamic* cost functionals as

$$\mathcal{J}^{\mathrm{stat}} \;=\; \sum_{j=1}^{N_\theta} J(k_{\min}, \boldsymbol{d}_j) \qquad \text{and} \qquad \mathcal{J}^{\mathrm{dyn}} \;=\; \sum_{j=1}^{N_\theta} \sum_{p=1}^{N_k} J^{\mathrm{dyn}}(k_p, \boldsymbol{d}_j), \tag{17}$$

and their sensitivities $\mathcal{D}\mathcal{J}^{\mathrm{stat}}$ and $\mathcal{D}\mathcal{J}^{\mathrm{dyn}}$ are computed by summing accordingly the sensitivities $\mathcal{D}J$ and $\mathcal{D}J^{\mathrm{dyn}}$ defined by (16).

3.3. Example: incorrectly manufactured chessboard-like material

The chessboard-like material, *as designed*, is depicted in the left panel of Fig. 2, featuring the coefficient ratios $\mu_{\max} = 7\mu_{\min}$ and $\rho_{\max} = 1.2\rho_{\min}$. For this configuration, the coefficients of homogenization are computed using the finite element platform FreeFem++ [3] as:

$$\begin{aligned} &\varrho^0 = 1.1\rho_{\min} && \boldsymbol{\mu}^0 = 2.65\mu_{\min}\boldsymbol{I} \\ &\boldsymbol{\varrho}^2 = 1.15\times 10^{-4}\rho_{\min}\boldsymbol{I} && \boldsymbol{\mu}^2 : \begin{cases} \mu^2_{1111} = \mu^2_{2222} = 4.36\times 10^{-3}\mu_{\min} \\ \mu^2_{1122} = 1.20\times 10^{-2}\mu_{\min} \\ \mu^2_{1112} = \mu^2_{1222} = 0 \end{cases} \end{aligned} \quad . \tag{18}$$

The chessboard-like material, *as manufactured*, has a defective top-left box in each unit cell, where $\mu = 4$ instead of $\mu = 7$ as shown in the right panel of Fig. 2.

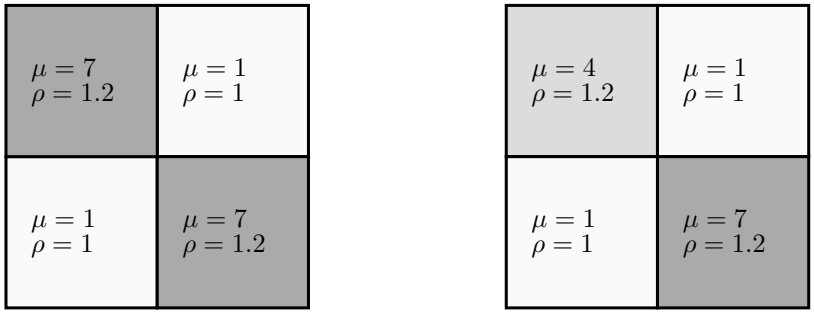

Figure 2: *Designed (left) and manufactured (right)* 1×1 *unit cell of a chessboard-like material.*

To identify and localize the defect, the plane-wave probing grid has $N_\theta = 3$ incident directions $(\theta_1, \theta_2, \theta_3) = (-\pi/4, -\pi/8, 0)$ and $N_k = 10$ wavenumbers $k_p = 2p\,\pi/30$, $p = \overline{1, N_k}$. With such hypotheses, the *shortest wavelength* used to probe the periodic structure is $\lambda_{\min} = 2\pi/k_{N_k} = 3$ which, relative to the 1×1 size of the chosen unit cell, implies sensing *below* the classical diffraction limit. With reference to the above sensing grid, the left panel in Fig. 3 compares the second-order approximation of the phase velocity (12) with the *numerical* values of $c(k, \boldsymbol{d})$ – as computed via Floquet-Bloch transform [5] – for both the designed and manufactured unit cell configuration. As can be seen from the display, the second-order approximation of anisotropic dispersion for the designed material agrees reasonably well with numerical simulations, noting that the small discrepancy between the two is attributed primarily to a limited accuracy of the numerical (Floquet-Bloch) solution due to a combination of material discontinuities inside the unit cell (which slow down the numerical convergence) and computer memory limitations. In contrast, there is a notable discrepancy between the dispersive characteristics of the designed and manufactured material, which justifies the use of the quasistatic functional $\mathcal{J}^{\text{stat}}$ (17) as a basis for (periodic) defect identification. From the results for $\Delta c(k, \boldsymbol{d})$ shown in the right panel of Fig. 3, this is also the case with the dynamic functional $\mathcal{J}^{\text{dyn}}$.

In this setting, the quasistatic sensitivity $\mathcal{D}\mathcal{J}^{\text{stat}}$ serves as an indicator of the relative stiffness of the manufactured material (stiffer or softer than the designed material), via the sign of $\Delta\mu$ which gives $\mathcal{D}\mathcal{J}^{\text{stat}} < 0$. In this vein, Fig. 4 plots $\mathcal{D}\mathcal{J}^{\text{stat}}(\boldsymbol{z})$ over the support of the unit cell, assuming both $\Delta\mu = 1$ (left panel) and $\Delta\mu = -1$ (right panel). To simplify the discussion, the analysis assumes prior knowledge of the fact that the mass density of the unit cell is manufactured exactly (see Fig. 2) by letting $\Delta\rho = 0$. For $\Delta\mu = 1$, we see that $\mathcal{D}\mathcal{J}^{\text{stat}} \geqslant 0$ everywhere; in other words, adding a stiff inclusion to the designed unit cell anywhere would only increase the quasistatic misfit functional. On the contrary, for $\Delta\mu = -1$ one has $\mathcal{D}\mathcal{J}^{\text{stat}} \leqslant 0$ everywhere

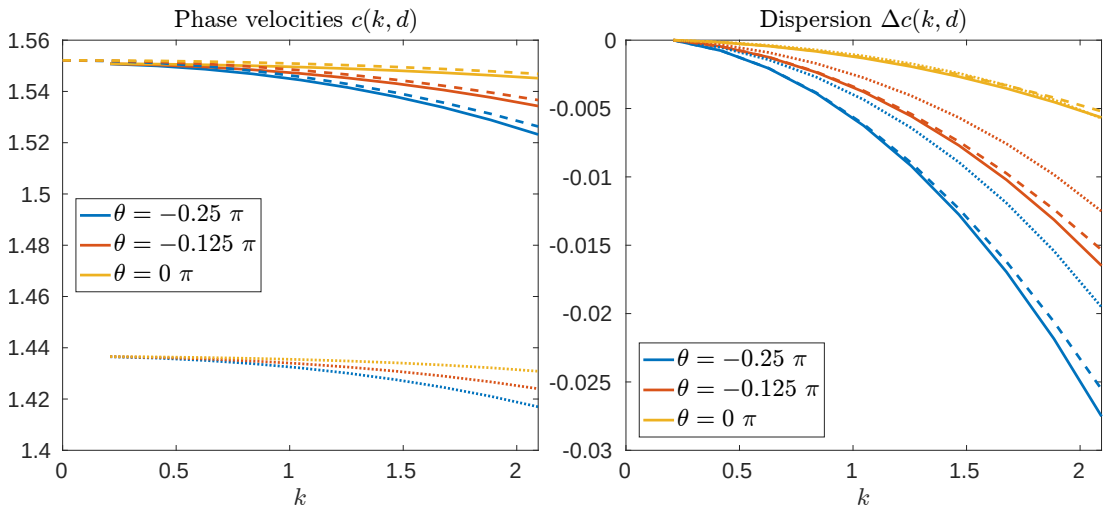

Figure 3: *Left: phase velocity* $c(k, \boldsymbol{d})$ *for the* designed *chessboard material (homogenized model - dashed, numerical values - solid), and* manufactured *chessboard material (numerical values - dotted). Right: anisotropic dispersion shown in terms of* $\Delta c(k, \boldsymbol{d}) = c(k, \boldsymbol{d}) - c(k_{\min}, \boldsymbol{d})$.

as expected since the manufactured material is *softer* than designed. In light of its sign semi-definiteness for given $\Delta\mu$, however, $\mathcal{DJ}^{\text{stat}}$ appears to have *no localizing capabilities* in that it cannot locate (even approximately) the support of a periodic defect inside the unit cell.

To tackle the latter drawback, we deploy the dynamic sensitivity $\mathcal{DJ}^{\text{dyn}}$ as a sensing lense in Fig. 5, taking $\Delta\mu = -1$ thanks to the quasi-static result. Indeed, the dynamic sensitivity appears to serve as a *remarkable defect locator*: $\mathcal{DJ}^{\text{dyn}} \geqslant 0$ over most of the intact quarter-cells – which are manufactured correctly (except near material interfaces, were the sensitivities tend to localize), while $\mathcal{DJ}^{\text{dyn}} \leqslant 0$ over the entire "defective" upper-left quarter-cell as expected, but also over the lower-right quarter-cell. The latter, however, should not be surprising, since (for the manufactured material at hand) the support of the unit cell could be chosen such that the defective quarter-cell appears as either upper-left or lower-right.

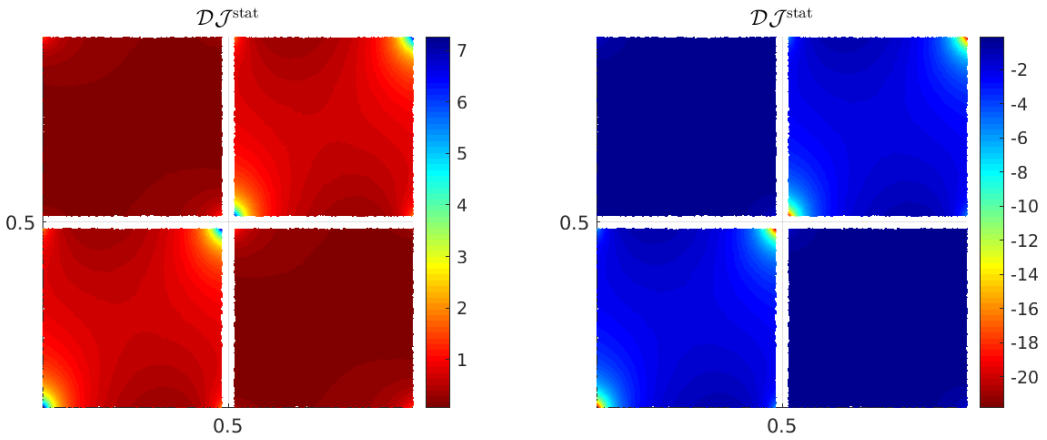

Figure 4: *Distribution of quasistatic sensitivity* $\mathcal{DJ}^{\text{stat}}(\boldsymbol{z})$ *over the unit cell assuming* $\Delta\mu = 1$ *(left) and* $\Delta\mu = -1$ *(right). The near-interface points are omitted from the plot.*

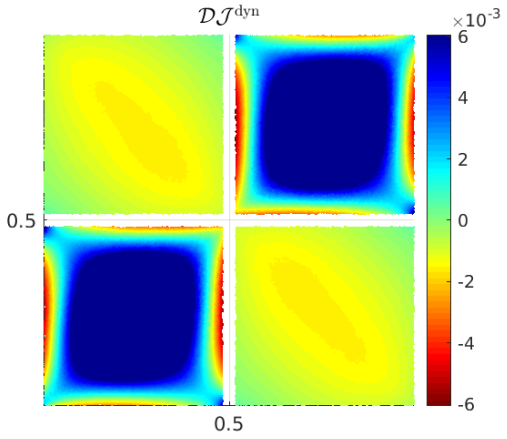

Figure 5: *Distribution of dynamic sensitivity $\mathcal{DJ}^{\mathrm{dyn}}(\boldsymbol{z})$ over the unit cell assuming $\Delta\mu = -1$. The near-interface points are omitted from the plot, and a threshold is applied to the most positive TS values (as only their sign is of interest).*

4. Summary and discussion

We derived the topological sensitivities of the coefficients of the wave equation obtained by second-order homogenization of a periodic material, with respect to the size of an inhomogeneity perturbing the unit cell that defines such material. These sensitivities are expressed in terms of (i) three unit-cell solutions used to formulate the unperturbed macroscopic model, (ii) two adjoint-field solutions driven by the mass density variation inside the unperturbed unit cell, and (iii) the polarization tensor, that synthesizes the geometric and constitutive features of the perturbation.

In light of the above results, the long-wavelength sensing of periodic defects or perturbations could be established by (i) considering the *anisotropic dispersion*-based cost functionals (17), (ii) choosing the sign of the stiffness contrast so that $\mathcal{DJ}^{\mathrm{stat}}(\boldsymbol{z}) \leqslant 0$ everywhere, and (iii) identifying the support of a perturbation inside the unit cell via regions where $\mathcal{DJ}^{\mathrm{dyn}}(\boldsymbol{z}) \leqslant 0$.

Reasonable levels of noise on the data should not alter the efficiency of the method, because (i) the cost functionals aggregate the measurements from several configurations, thus an averaging effect, (ii) the topological sensitivities (16) are linear with respect to the data and therefore to the noise and (iii) only the sign (and not the values) of these sensitivities are of interest.

Finally, the choice of illumination by plane waves enabled to retain the phase velocity as a dispersion indicator. If such configuration cannot be reached in practice (e.g. because captors are too close from a source transducer for the plane wave approximation to hold), one should use another indicator to measure the dispersive properties of the material and define new cost functionals accordingly.

References

[1] Ammari H, Kang H and Touibi K 2005 Boundary layer techniques for deriving the effective properties of composite materials. *Asymptot. Anal.* **41** 119–140
[2] Bonnet M 2009 Higher-order topological sensitivity for 2-d potential problems. Application to fast identification of inclusions. *Int. J. Solids Struct.* **46** 2275–2292
[3] Hecht F 2012 New development in FreeFem++. *J. Numer. Math.* **20** 251–265
[4] Giusti SM, Novotny AA and de Souza Neto EA 2010 Sensitivity of the macroscopic response of elastic microstructures to the insertion of inclusions. *Proc. Roy. Soc. London. Series A.*
[5] Wautier A and Guzina BB 2015 On the second-order homogenization of wave motion in periodic media and the sound of a chessboard. *J. Mech. Phys. Solids* **78** 382–404